We are IntechOpen,
the world's leading publisher of Open Access books
Built by scientists, for scientists

4,000
Open access books available

116,000
International authors and editors

120M
Downloads

154
Countries delivered to

Our authors are among the

TOP 1%
most cited scientists

12.2%
Contributors from top 500 universities

BOOK CITATION INDEX
CLARIVATE ANALYTICS
INDEXED

WEB OF SCIENCE™

Selection of our books indexed in the Book Citation Index
in Web of Science™ Core Collection (BKCI)

Interested in publishing with us?
Contact book.department@intechopen.com

Numbers displayed above are based on latest data collected.
For more information visit www.intechopen.com

Crystallography of Precipitates in Metals and Alloys: (1) Analysis of Crystallography

Yoshitaka Matsukawa

Abstract

This chapter and the following chapters describe crystallography of second-phase precipitate particles in metals and alloys. The focus of this chapter is placed on technical aspects in the analysis of their crystal structure, composition, and crystal orientation relationship with the matrix. Characterization of fine precipitates embedded in solid matrix is technically rather difficult; the signal from the matrix always hinders the signal from the precipitates. Although even state-of-the-art characterization techniques are still incomplete, it is becoming possible to assess the validity of assumptions involved in classic theories related to the crystallography of precipitates. For instance, recent experimental studies demonstrated that evolution of their crystal structure during nucleation seems to contradict the so-called classical nucleation theory, in terms of fluctuations in size and composition. Recent studies also demonstrated that their crystal orientation relationship with the matrix is often different from the one predicted by energy considerations related to the interfacial lattice mismatch. Furthermore, crystal orientation relationship with the matrix was found to be a factor controlling the magnitude of precipitation hardening, contrary to the conventional Orowan's hardening model based on continuum elasticity theory calculations without considering crystallography.

Keywords: precipitates, nucleation, crystal structure, strength, dislocations

1. Introduction

This chapter and the following chapters review recent progress of our knowledge about crystallography of precipitate particles in metals and alloys [1–3]. The main focus is placed on the following three subjects:

1. Evolution of crystal structure during nucleation

2. Crystal orientation relationship with the matrix

3. Effect of crystallography of precipitates on mechanical properties

These subjects are closely related to the following three basic theories, each of which has a long history greater than a half century:

1. The theory of crystal nucleation (since 1876) [4]

2. The theory of dislocations (since 1934) [5–9]

3. The theory of precipitation hardening (since 1954) [10, 11]

From an engineering viewpoint, the knowledge provided here is primarily useful for developing stronger materials. Dispersing fine precipitate particles over the matrix at high density is a common engineering technique for improving the strength of metals and alloys. By introducing a minor amount of second-phase precipitate particles, such as 2% in volume fraction, the material strength is increased by several times greater. In the traditional theory of precipitation hardening (a.k.a. dispersion strengthening) established in the 1950s–1960s, the primary factor controlling the magnitude of strengthening effect is assumed to be the shear modulus [10, 11], whether or not precipitates are harder than the matrix. This concept has been partly revised in the past few years. Recent experimental studies using state-of-the-art material characterization techniques demonstrated that crystallography of precipitate particles is another factor dominating their obstacle strength [1, 2]. When the slip plane of dislocations in precipitates is not parallel to that in the matrix, dislocations are unable to cut through the precipitates, resulting in large hardening, regardless of the shear modulus. This subject is extensively discussed in the next chapter.

This chapter may also be of interest for the audience outside of the research community of materials science and solid-state physics. Nucleation is one of the areas of basic science related to a wide variety of research subjects including chemical reactions in liquid and gas. In fact, the first theory was originally developed for the nucleation of droplets from gas. Nucleation of crystals in solid is more complicated than the situation assumed in liquid and gas, in a sense that the formation of a new crystal is highly constrained by the surrounding matrix, in terms of the strain energy associated with the precipitate/matrix interface and the diffusivity of atoms for their agglomeration. A long-standing open question is the critical condition for nucleation regarding size and composition of nucleus. Precipitates are in many cases compounds consisting of multiple elements such as carbides and oxides. Unlike in gas and in liquid, the diffusivity of each element is not the same in solids [12]. For instance, the diffusivity of light elements like carbon and oxygen is several orders of magnitude greater than that of metallic elements. Although the classical nucleation theory assumes that the crystal structure and composition of precipitates are the same as those of the final product from the beginning of embryo growth (**Figure 1**), the diffusivity difference indicates a possibility that the composition of precipitates fluctuates during the nucleation process. The classical nucleation theory also assumes that nucleation occurs when the embryos have grown up to a critical size. In many cases the critical size of precipitates for nucleation is 2–3 nm [3]. Assessing the composition of such small precipitates has been technically impossible until recently. The highlights of recent studies are discoveries that, in the early stage of precipitation, the crystal structure and composition of precipitates are different from those of the final product and that the precipitates structurally transform into the final product at a critical size with a critical composition (**Figure 1**). Precipitates are clusters of solute elements when they start spontaneous growth, which is defined as the state of "nucleation" in the classical nucleation theory. An implication of this finding is that the obstacle strength of precipitates in precipitation hardening may change during precipitation. They are weak obstacles in the early stage of precipitation regardless of the crystal structure of the final product. They can become strong obstacles due to a change in the shear modulus or
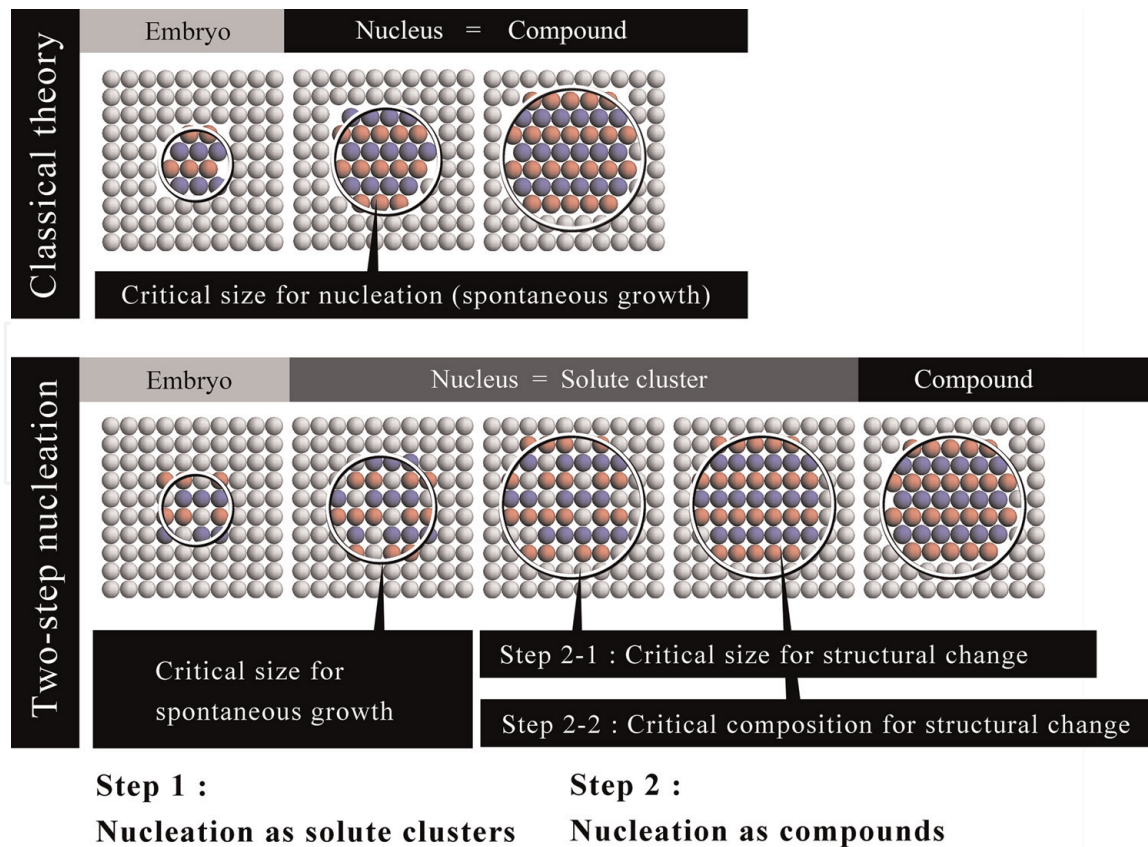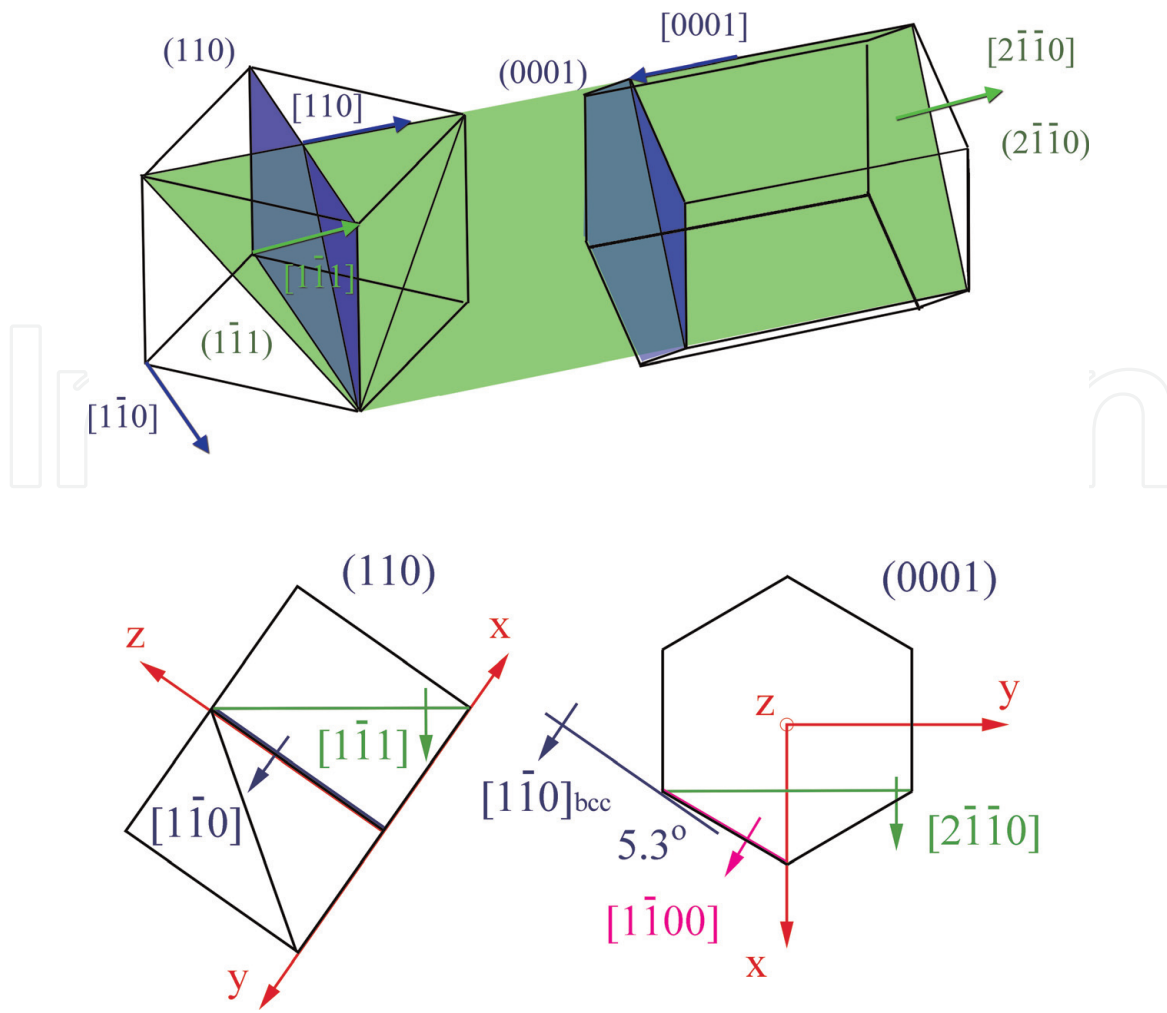
Figure 1
Nucleation of precipitates in metals and alloys: classical nucleation and two-step nucleation [3]. Unlike the classical nucleation theory, in reality, crystal nuclei do not emerge directly from the matrix. They first nucleate as solute clusters structurally indistinguishable from the matrix, followed by a structural change. Their crystal structure changes at a critical size with a critical composition.

the crystal structure. In some cases, precipitates become brittle by the structural change, while they are ductile in the state of solute clusters. Brittle precipitates are considered to serve as the nucleation site of cracks via particle cracking. Hence, from the viewpoint of fracture mechanics, the ductile-brittle transition of precipitates during precipitation considered a factor controlling the engineering lifetime of materials.

As a result of the constraints from the surrounding matrix, precipitation of the second phase often occurs with a specific crystal orientation relationship with the matrix. Precipitates and matrix share a specific atomic plane in such a way to minimize the mismatch between them. The orientation relationship is dependent on their crystal structure. For instance, in the Burgers orientation relationship, bcc precipitates in hcp matrix share atomic planes as follows (**Figure 2**) [13]: $(0001)_{hcp}//(110)_{bcc} \wedge (2\bar{1}\bar{1}0)_{hcp}//(1\bar{1}1)_{bcc}$. Since the lattice parameter is specific to materials, a preferable orientation relationship changes depending on the degree of mismatch of lattice parameter between precipitates and matrix. The Burgers orientation relationship is the optimum configuration for the combination of bcc pure Zr and hcp pure Zr, but another orientation relationship is preferred for the bcc Nb precipitates containing a few amount of Zr. The Zr-Nb binary system is a complete solid solution in a bcc structure at high temperatures [14]. The difference of lattice parameter between the bcc Zr and the bcc Nb is ~10% [15]; the lattice parameter of bcc precipitates changes in accordance with Vegard's law [2]. Apart from a remarkable progress in theoretical works on the orientation relationships, experimental studies have recently demonstrated that precipitates and matrix do not always follow such a theoretically predictable, ideal orientation relationships in reality. Recent analysis using electron backscatter diffraction (EBSD) (**Figure 3**)
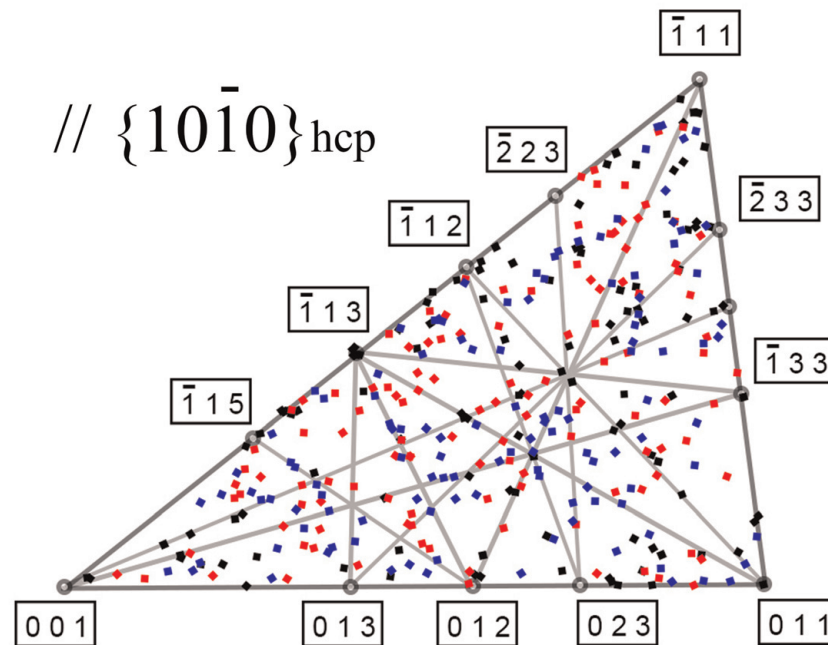
Figure 2
The Burgers orientation relationship for bcc and hcp crystals [2]. This is the most traditional orientation relationship discovered in 1934.

Figure 3
Example of EBSD analysis of precipitates: bcc Zr precipitates containing Nb and hcp Zr matrix in a Zr–2.5Nb alloy [2].

revealed that, when the matrix undergoes recrystallization after precipitation of precipitates, their orientation relationship is overwritten. As a result of that, crystal orientation of precipitates can become random (**Figure 4**). The degree of

Figure 4
EBSD analysis results of atomic planes of precipitate particles parallel to the slip plane of matrix: bcc Nb precipitates and hcp Zr matrix in a Zr–2.5Nb alloy [2]. Only 1 out of 100 precipitate particles had a slip plane parallel to that of the matrix. Hence, dislocations are unable to cut through the bcc Nb precipitates.

contribution of precipitates to the strength of materials may become different from what is expected from well-known crystal orientation relationships [2].

Recent updates of these theories have been achieved by progress in material characterization methods for determining the crystal structure and composition of nano-sized precipitates. Before going into the details of these theories, we briefly review the technological breakthrough in experimental methods. This chapter is addressed to not only the specialists of precipitates but also nonspecialists including students. For better understanding, traditional methods of material characterization are also briefly reviewed at the beginning.

2. Brief history of microstructure characterization techniques

Crystal structure is determined based on the concept of diffraction, discovered in 1912. It appears that X-ray diffraction (XRD) became common in the 1920s; a great many structures of alloys were determined. Early works determined simple structures having a high symmetry with which peaks in the XRD spectrum are clearly resolved free from overlapping. Precipitates are, however, in many cases compounds having a low symmetry. XRD became applicable to such complicated structures by the invention of the Rietveld method in 1966 [16]. Precipitates involved in bulk metallic samples are detectable only when their volume fraction is higher than ~1% [17], though that is highly dependent on their crystal orientation relationship with the matrix. In bulk samples the crystal orientation of precipitates is not necessarily random, and the matrix grains also not. Metallic bulk samples cannot be crushed into powders due to their high ductility. They can be mechanically grinded into powders by using a hand grinder; however, the XRD peaks of such grinded metallic powders are broadened due to introduction of dislocations,

resulting in hindering the peaks of precipitates by the background noise. These issues are avoided by the use of residue extracted from the matrix via chemical dissolution using an acid [18]. This extraction residue analysis is, however, applicable to only nonmetallic compound precipitates embedded in metallic matrix.

Transmission electron microscope (TEM) is a multifunctional characterization tool capable of determining not only crystal structure but also composition and size of precipitates on the image of microstructure, free from the constraint due to volume fraction. The first prototype was produced by Ruska et al. in 1932, and the first commercial model was released by Siemens in 1939. It appears that TEM became common in the 1950s; for example, the number of commercial products released in Japan was greater than 250. The resolution (point resolution) was 50 nm for Ruska's first TEM, 1 nm for the Siemens Elmiskap I released in 1956, and 0.2 nm for the JEOL JEM100B released in 1968. Precipitates are visualized using diffraction contrasts; those satisfying the Bragg condition exhibit dark contrast in the so-called bright-field image (bright contrast in the dark-field image), whereas the others are indistinguishable from the matrix. The number density of precipitates determined by diffraction contrast images represents the true number density only in the case where precipitates are all aligned to the same crystal orientation. This condition is achievable only when precipitation occurs with a specific crystal orientation relationship with the matrix such as the cube-on-cube orientation relationship, where the unit cells of the precipitate and the matrix completely overlap each other. In the other orientation relationships, some crystallographic variants are often invisible. This is a potential error in the evaluation of the number density of precipitate particles but often out of consideration. In many cases, the magnitude of error bars is determined solely by a statistical analysis: either the standard error or standard deviation.

High-resolution (HR)-TEM is another mode capable of visualizing precipitates using phase contrasts, i.e., lattice fringes generated by interference of transmitted and diffracted electron waves. This imaging mode became common in the 1970s–1980s [19]. In those days, however, alignment of electron beam axis was technically difficult for entry-level users. This technical issue was resolved in the 1990s by an introduction of the field-emission gun, which provides a hundred times brighter illumination, a digital camera system, a real-time image processing software (fast Fourier transformation for the alignment minimizing the objective lens stigmatism), etc. However, even though the issue of beam alignment has been resolved, HR-TEM analysis of nano-precipitates is still extremely time-consuming due to alignment of crystal orientation. The HR-TEM image (crystal lattice image) is obtained only when the direction of incident electron beam is aligned with the crystal's zone axis having a low index, e.g. [001] and [110]. The beam-crystal alignment, achieved by using Kikuchi lines or bend counters, is easy for large precipitates greater than several hundred nm but technically almost impossible for nano-precipitates. So for this reason, in practice, the operator searches particles which already exhibit the crystal lattice image without tilting the sample. Unless otherwise precipitates have a specific orientation relationship with the matrix, the operator can find only a few but not many such particles, whereas the minimum requirement of the number of precipitates for drawing a smooth histogram of the size distribution is ~500 in the author's experience [3].

TEM is capable of determining the crystal orientation relationship between precipitates and matrix, though this analysis is also extremely time-consuming. In order to determine the orientation relationship, one needs to find out a sample-tilting angle, where the beam direction is aligned with a zone axis. Three such tilting angles need to be found for both precipitates and matrix in order to determine their (hkl) indices. In some cases precipitates may not have any specific orientation

relationship with the matrix; however, proving such a random orientation relationship is practically impossible for one-to-one analysis using a TEM. The random orientation issue can be assessed only if the number density of precipitates is sufficiently high enough for obtaining the Debye ring patterns in selected-area electron diffraction. A more appropriate method rather than TEM to investigate this research subject is EBSD equipped on a scanning electron microscope (SEM). EBSD determines the orientation of crystals based on the Kikuchi pattern, whose theoretical accuracy is ∼0.1° [20, 21], whereas the accuracy of orientation analysis using diffraction spots is ∼3° [22, 23].

The first report introducing the principle of EBSD was published in 1973, within 10 years after the release of the first commercial SEM, the Stereoscan series 1, by the Cambridge Instrument Company in 1965. EBSD became a practically useful tool in 1993, by full automation of mapping (detecting, indexing, and recording the Kikuchi bands based on the Hough transformation). The spatial resolution of EBSD is dependent on probe size, step size of scanning, accelerating voltage of electrons, sample geometry (bulk or thin foil), etc. According to the author's experience, precipitates of ∼500 nm in diameter can be identified but ∼50 nm not. The spatial resolution is improved by using an advanced technique called transmission Kikuchi diffraction (TKD), a.k.a. transmission EBSD, proposed in 2012 [24]. This new technique works on conventional EBSD system and software. The difference is that TKD uses forward-scattered electrons, whereas EBSD uses backscatter electrons. In other words, TKD uses transmitted electrons as well as TEM; hence, the samples must be thin foils. Sample preparation is not difficult for TEM users; TEM samples can be directly subjected to this analysis. The high spatial resolution of TKD owes not only to the use of thin foil specimens, which minimize unfavorable lateral beam spreading inside the specimens, but also to a greater signal intensity of forward-scattered electrons than backscattered electrons [25]. Since the Kikuchi pattern is generated from elastic scattering (diffraction) of inelastically scattered electrons [26], there exists a lower limit in both specimen thickness and precipitate size below which the Kikuchi patterns are not obtained. When the thickness of thin foil specimens is largely greater than the size of precipitates, the signal from the precipitates is hindered by that from the matrix. In other words, there exists an upper limit of measurable foil thickness depending on the size of precipitates. Only a limited range of thickness is applicable to this method in a wedged-shaped TEM thin foil specimens. The practical spatial resolution limit of TKD is dependent on many factors such as the position of detector (florescent screen); according to the author's experience using a conventional EBSD system, precipitates of ∼50 nm in diameter can be identified but ∼10 nm not. The resolution will be improved if the detector is placed just beneath of the sample; this is an ideal setting that minimizes the loss of forward-scattered electrons.

Traditionally, TEM has been a primary analysis tool for composition analysis of precipitates: energy-dispersive X-ray spectroscopy (EDS) and electron energy loss spectroscopy (EELS). In these TEM-based composition analyses, samples having a 3D geometry are projected on 2D space via electron transmission. Precipitates often overlap the matrix in the thickness direction, whereas their TEM image is constructed based on integrated information over thickness. These analyses are unable to determine the composition of overlapped portion. It is practically impossible to judge from the projected 2D image if the precipitates are free from overlapping. In terms of composition analysis of precipitates, the most innovative breakthrough in the past two decades is probably the invention of atom probe tomography (APT). Although its concept was first proposed in 1967, it has become a practically useful tool since the commercial release of local-electrode atom probe (LEAP) in 2003. APT is capable of visualizing atoms in 3D space, which is a critical advantage over the TEM-based composition analyses. APT is a quantitative mass

analysis, whereas EDS and EELS are semiquantitative analyses that require a standard sample for calibration. Furthermore, EDS is inherently lack of quantitative accuracy in detection of light elements; emission of Auger electrons is dominant over characteristic X-ray and is dominant for low-Z elements like oxygen. Although APT is superior to TEM-based analyses in many aspects, determination of precipitates' composition is a challenging subject even for APT. The quantitative precision of the APT composition analysis is often limited by artifacts partly due to the so-called trajectory aberration [27–29]. For precipitates darkly imaged in FIM (i.e., low evaporate field regions) compared to the surrounding matrix, defocused high-field iron ions coming from the surrounding matrix fall into the precipitate image on the detector [30]. Conversely, for precipitates brightly imaged in FIM, image overlapping occurs outside the precipitate image. In both cases, mixing with the matrix elements inevitably occurs at the interface. Hence, matrix elements are often detected in nano-precipitates [31, 32].

3. Evolution of crystal structure during nucleation

The classical nucleation theory is based on the so-called capillarity approximation, which assumes that the properties of nuclei are the same as those of the final product from the beginning of embryo growth. In other words, all parameters that characterize the new crystal phase to be distinct from the matrix phase, such as density, composition, and structure, are assumed to be unchanged throughout the nucleation stage. Under this assumption, nucleation event is expected to be solely controlled by the size of embryos. Spontaneous growth (nucleation) of precipitates is expected to occur at a critical composition where the hierarchy of the bulk free energy of the precipitate phase and the surface free energy of precipitate/matrix interface is reversed. In the past two decades, a modern concept called the two-step nucleation has been established by the research community of crystal nucleation
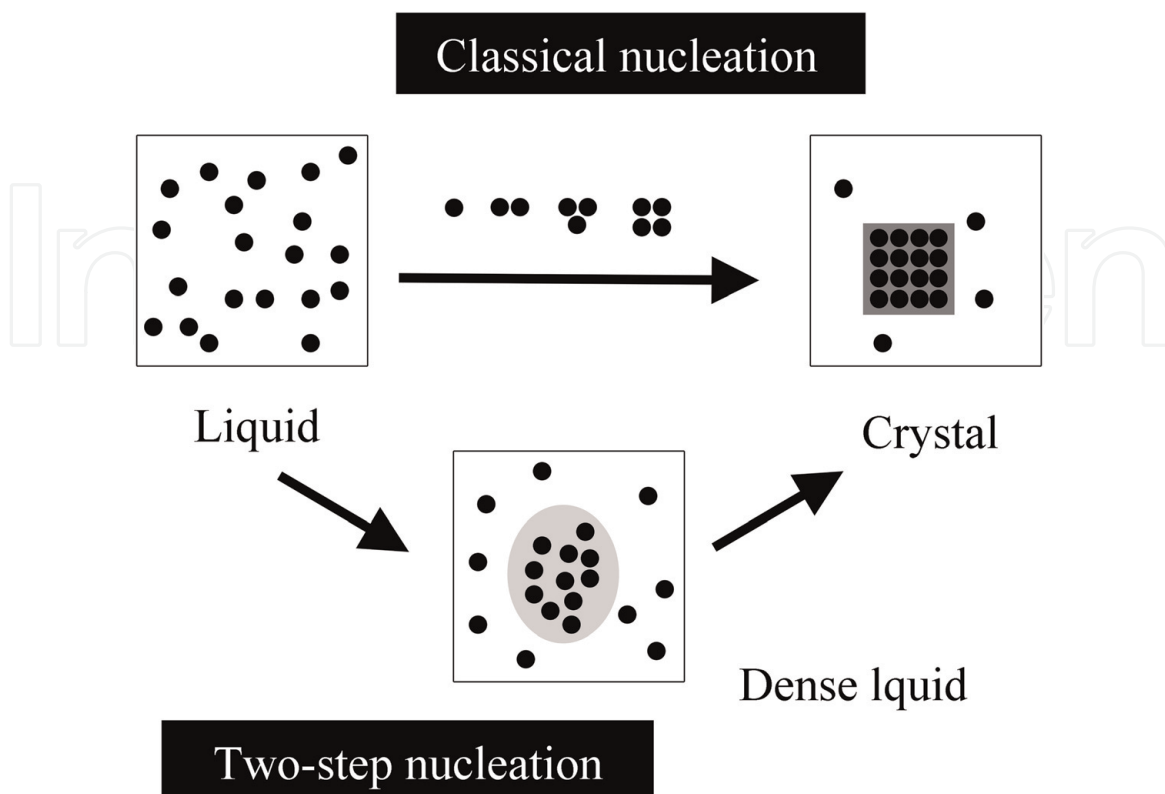
Figure 5
Two-step nucleation of crystals from liquid [33].

from liquid (**Figure 5**) [33]. This concept is nonclassical in that embryos become distinct from the matrix liquid in terms of density prior to the structural change. Here, fluctuation of composition is generally out of consideration, as in liquid diffusivity of solute elements is equally very high; composition fluctuation is expected to be negligibly small. On the other hand, in the nucleation of compound precipitates in crystalline solids, fluctuation of density is relatively small (compared to the nucleation of solid from liquid), but instead, composition may be a variable parameter. In solids, diffusion coefficients of solute elements are merely the same; stoichiometric composition of the compound may not be fulfilled in the early stage of embryo growth. In this case, although the parameter being in focus is different from the conventional two-step nucleation in liquid, this is also nonclassical in the sense that multiple parameters required for nucleation evolve in parallel during nucleation. In 2014, Peng et al. demonstrated that a solid-solid phase transition occurs in a two-step process [34]. In their experiments using a model crystal consisting of microgel colloidal spheres, the two-step represents a two-step change in structure. The first step is a transition from a two-dimensional square lattice structure to a liquid-like structure, and the second step is a transition from the liquid-like structure to a two-dimensional triangular lattice structure. Fluctuation of composition is not associated with their two-step process. Within the framework of the classical nucleation theory, in 1937 Borelius assumed that composition is a variable parameter in the nucleation of precipitates in solids [35]. Absolute value of the bulk free energy of precipitates becomes the greatest with the compound's stoichiometric composition; nucleation is expected to occur at this critical composition. Borelius did not discuss the effect of compositional fluctuation on the critical size. In 1949, Hobstetter attempted to handle both size and composition as variable parameters [36]. He demonstrated that in this two-variable analysis there is a pathway (in terms of evolution of size and composition) energetically more favorable than the pathway fixed by the previous one-variable analyses. However, the meaning of the energetically most favorable pathway remained unclear in the context of critical size and composition.

The final product described in the classical nucleation theory is not necessarily the most stable, equilibrium phase. In many cases, the first nucleating phase is a metastable phase, formation of which occurs with the lowest energy barrier; the equilibrium phase is produced through multiple transitions from a metastable phase to another metastable phase step-by-step. This is an empirical rule known as Ostwald's rule of stages, proposed in the 1890s [37, 38]. One of such examples is precipitation of Al_2Cu at Guinier-Preston (GP) zone in Al-Cu alloys [39, 40]. The precipitation of Al_2Cu, which is the stable phase in this system, is known to occur via multiple intermediate configurations such as GP zone → coherent θ" phase → semi-coherent θ' phase → incoherent θ phase (Al_2Cu). Those intermediate phases are distinct from the Al_2Cu in both crystal structure and composition. Another example is precipitation of fcc Cu in bcc Fe matrix. Precipitation of Cu is known to occur via multiple intermediate configurations such as bcc Cu → a twinned 9R Cu → fcc Cu [41]. The bcc Cu precipitates are crystallographically indistinct from the matrix; in other words, they are solute clusters in the bcc solid solution. The critical composition for their structural changes remains unclear. It is technically rather difficult to determine the composition of precipitates in the early stage of precipitation due to their small sizes.

Traditionally, experimental studies on the nucleation in solids have focused on determining the critical size. For example, Othen et al. [41] reported that the bcc Cu precipitates grow with the twinned 9R structure in a size range from 6 to 15 nm. Their conclusion is based on the results of HR-TEM observation. This methodology is, however, insufficient for statistical argument as mentioned in the previous section.

Even today, experimental studies on the critical composition for nucleation are still limited. As mentioned earlier, even in atom probe tomography, mixing with matrix elements inevitably occurs at the precipitate/matrix interface due to trajectory aberration. Hence, it is practically impossible to judge if the abovementioned Cu precipitates embedded in Fe matrix is 100% pure Cu. When the precipitate of interest is a compound consisting of multiple elements, the ratio of its constituent elements can be discussed. However, when one of those elements is the element of matrix, such as the Al–Cu precipitates in Al alloys, interpretation of their concentration ratio is not straightforward.

In order to determine the critical composition for the structural change, the crystal structure of precipitates must be examined together with composition. In TEM observation of diffraction contrasts, precipitates are indistinguishable from the matrix while they are solute clusters, and they become visible after structural change. By using this unique feature in visibility, recently, Matsukawa et al. performed a systematic analysis on the precipitation of the G-phase in a duplex stainless steel subjected to thermal aging [3]. The crystal structure of the G-phase is cF116 (a variant of fcc structure), and the lattice parameter is exactly fourfold of the matrix ferrite (**Figure 6**). Precipitation occurs with the cube-on-cube orientation relationship [42]. The stoichiometric composition is $Ni_{16}Si_7Mn_6$; its constituent elements are different from the matrix elements (Fe and Cr). So for these reasons, this intermetallic compound is ideal for the fundamental study of nucleation. Precipitation of G-phase in duplex stainless steels is known to occur only in a very narrow temperature range, 673–773 K [43]. In their study, thermal aging was performed at 673 K for up to 10,000 h.

Their analysis revealed that precipitation of Ni–Si–Mn clusters started at 500 h (**Figure 7**), whereas their structural change transforming into the G-phase started at 10,000 h (**Figure 8**). The number density of G-phase particles detected by TEM was only ∼26% of the number of Ni–Si–Mn precipitates detected by APT. In other words, three quarters of the Ni–Si–Mn precipitates were solute clusters yet without structural change. The number of particles examined by TEM was ∼750. A potential error factor that could cause a misevaluation of the precipitate number density is the method used to evaluate the thickness of the TEM foil. Their method was to use thickness fringes obtained at an exact Bragg condition, where the deviation parameter was s=0. In this case, thickness is determined by the number of thickness fringes multiplied by the extinction distance of the electron beam. Since the precipitate number density was counted in portions where the number of thickness fringes was 4, the magnitude of the error in the foil-thickness evaluation was ±25%. In other words, the number of Ni–Si–Mn clusters that exhibited the crystal structure change was at most 50% of the total.

Their APT analysis also revealed that the Ni–Si–Mn clusters contained not only the G-phase elements (Ni, Si, and Mn) but also the matrix elements (Fe and Cr) and that enrichment of the G-phase elements occurred during thermal aging. Unlike the size growth, the solute enrichment continued even after 5,000 h. In the composition analysis of the clusters (**Figure 9**), those clusters were divided into three groups by size, i.e., small (<2 nm in diameter), medium (2–3 nm), and large (>3 nm), in order to minimize the artifacts that occur at the cluster/matrix interface; a comparison of cluster composition should be made for those having the same size. The concentration ratio of the G-phase elements (Si/Ni and Mn/Ni) did not change during the isothermal aging. The Mn/Ni ratio was in good agreement with that of stoichiometric composition, whereas the Si/Ni ratio was roughly a half of the stoichiometric ratio.

Their analysis indicates that the nucleation of the G-phase occurred via a two-step process: the first step is the spontaneous growth of solute clusters (i.e., nucleation as solute clusters), and the second step is the nucleation as compounds (i.e., the G-phase) (**Figure 1**). There was a time lag between the end of size growth
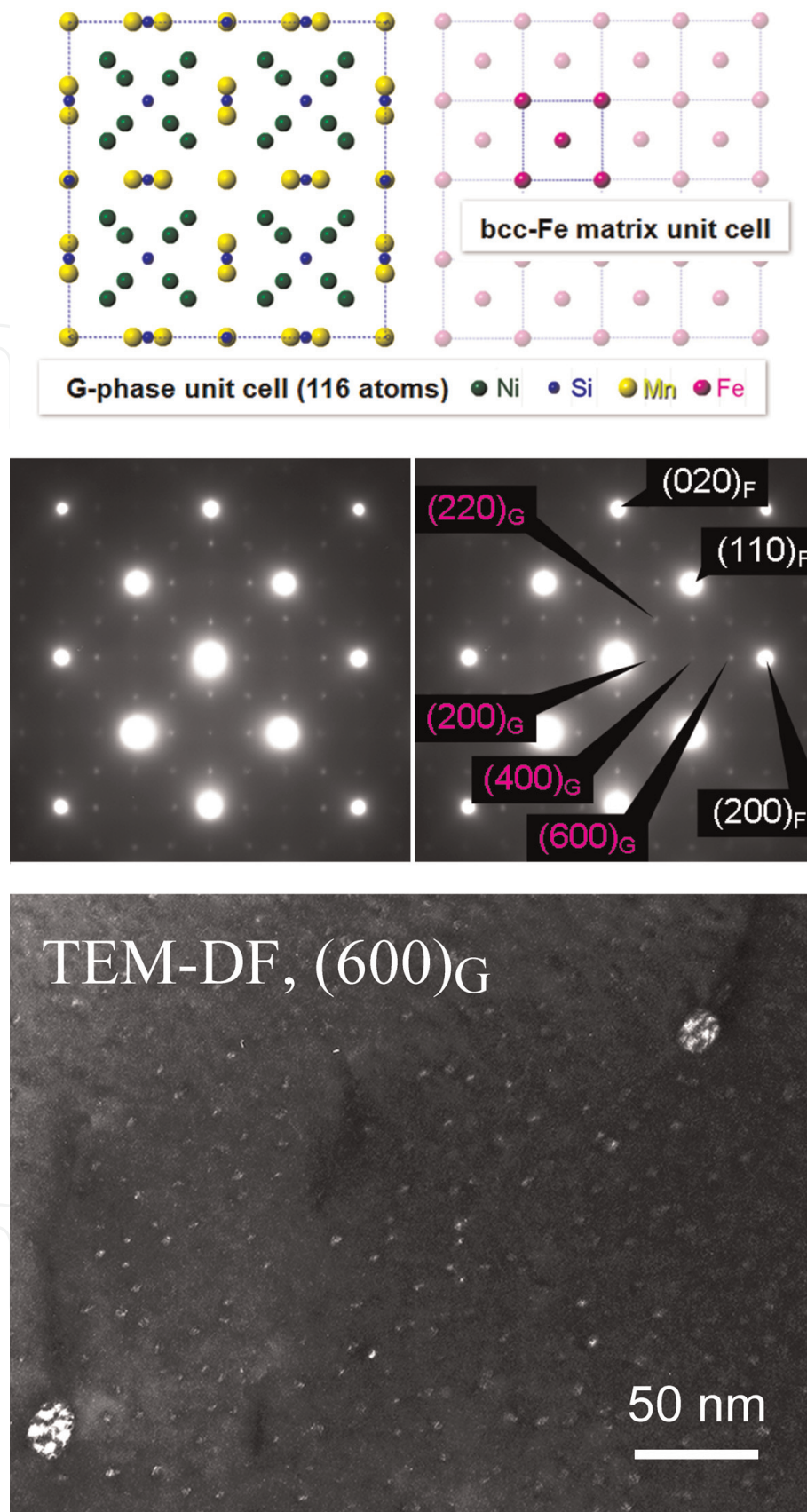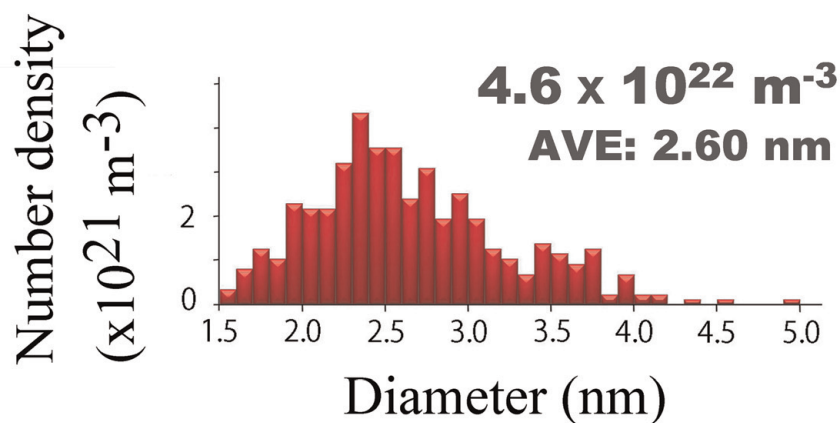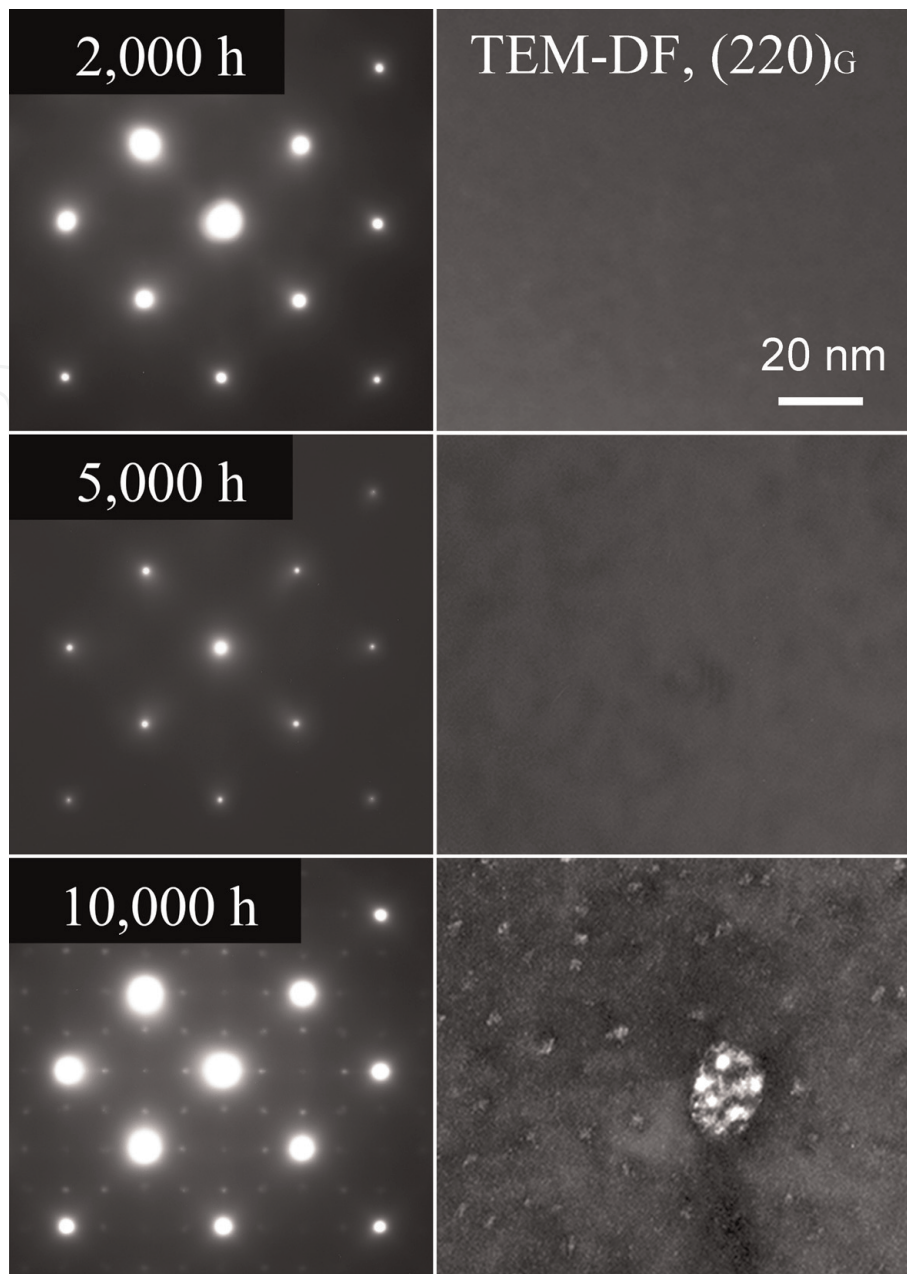
Figure 6
Crystal structure and TEM electron pattern of the G-phase precipitates in the ferrite portion of a duplex stainless steel subjected to thermal annealing at 673 K [3].

(5,000 h) and the start of structural change (10,000 h). It appears that the incubation period was controlled by solute enrichment inside the clusters. In other words, the structural change occurred via another two-step process: the first step is size fluctuation to become a critical size, and the second step is composition fluctuation to become a critical composition (**Figure 1**).
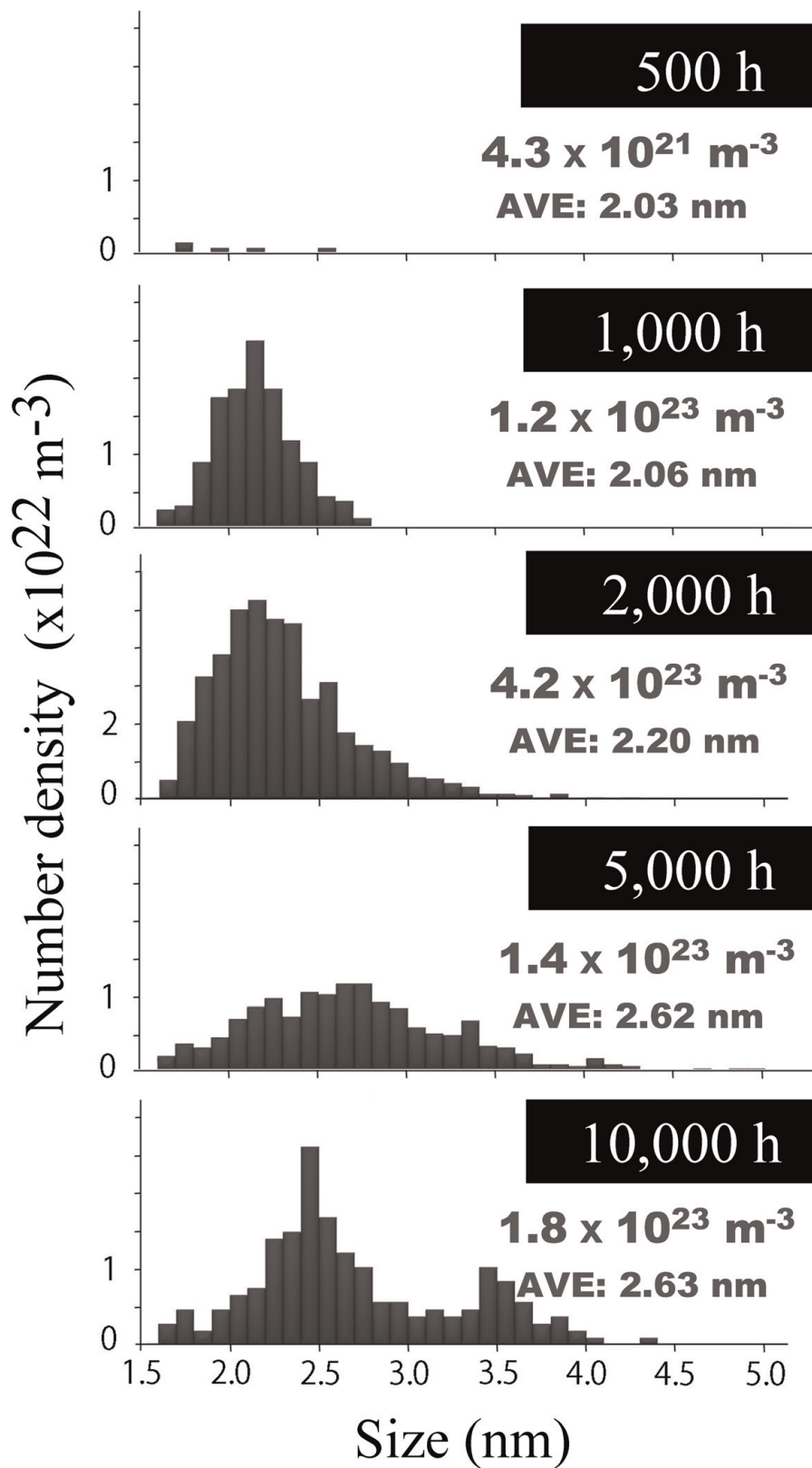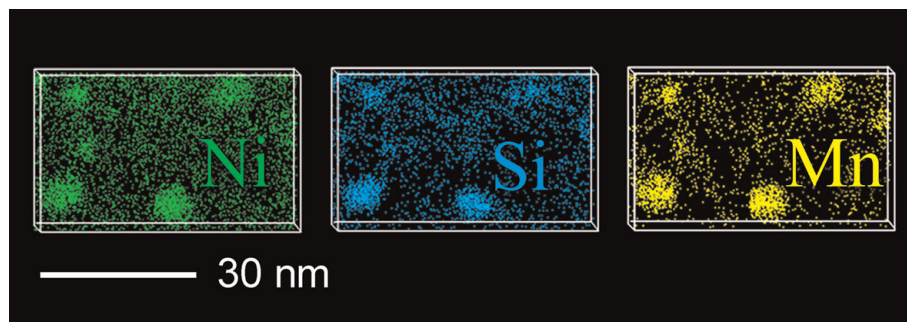
Figure 7
APT results on the steel [3]: size and number density of Ni–Si–Mn clusters.

Figure 8
TEM results on the steel [3]. The G-phase precipitates were detected by diffraction pattern and DF image, only in the sample annealed up to 10,000 h. Their number density was only ~26% of the Ni–Si–Mn clusters detected by APT.

The G-phase is currently of particular interest in nuclear materials research, as this compound precipitates also in the steel constituting the main body of reactor pressure vessels (RPVs) at the operation temperature of light water reactors
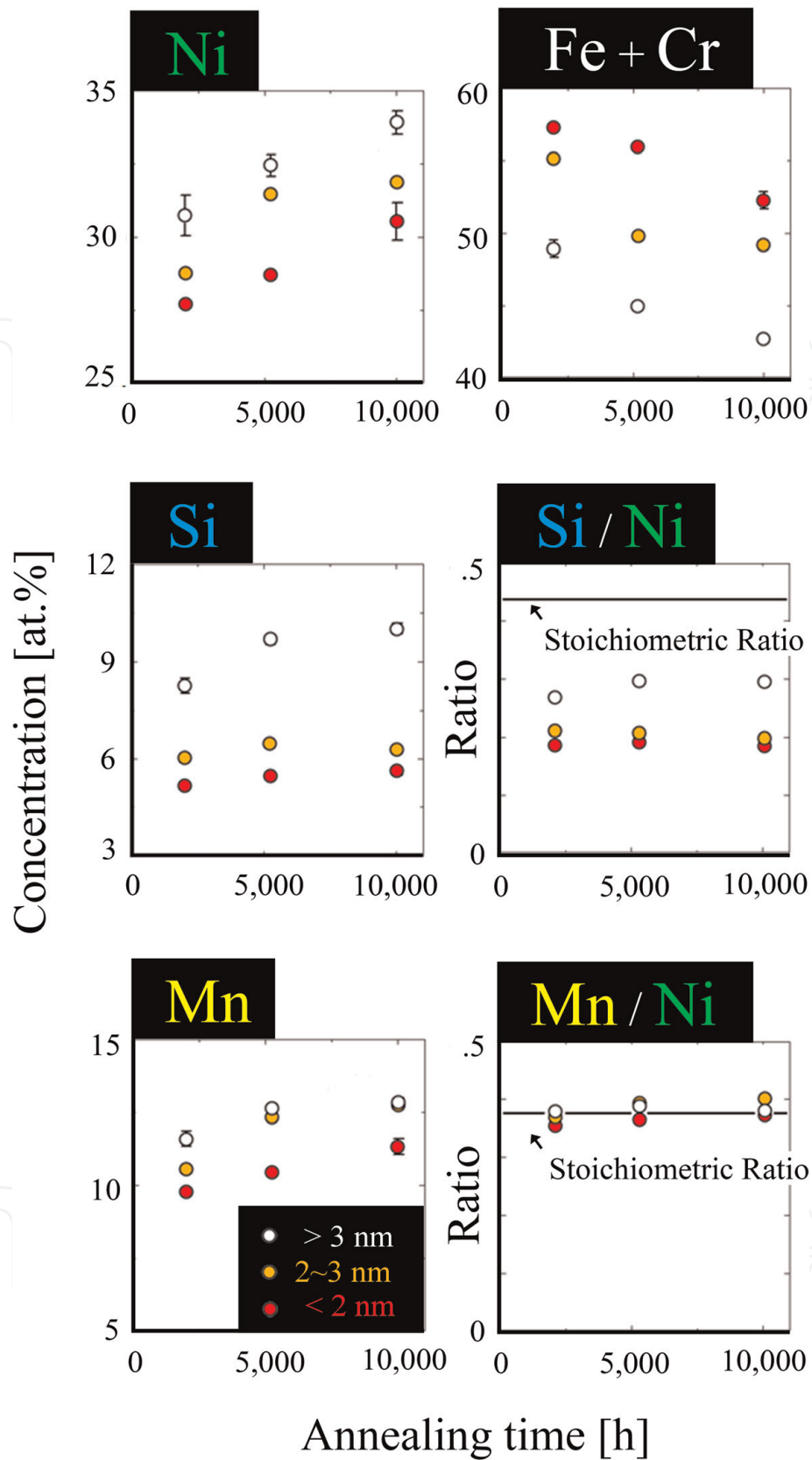
Figure 9
APT results on the steel [3]: composition of Ni–Si–Mn clusters.

(∼573 K) under neutron irradiation. It has long been well known that precipitation of impurity Cu causes embrittlement of the RPV steels. In the late 1990s, Odette et al. pointed out that, in the case of RPV steels containing a low amount of Cu such as those manufactured after 1973, precipitation of Cu occurs in the first few years of reactor operation, but near the end of the plants' initial operational license lifetime

(typically 40 years), precipitation of Ni, Mn, and occasionally Si becomes dominant over Cu [44]. The Ni–Mn(–Si), precipitates have been called the late-blooming phase [45–47] since their structural and compositional features were unclear at that time. It was very recently that the late-blooming phase is in many cases found to be characterized as the G-phase [48, 49]. The composition of the late-blooming phase detected by APT is not always the same [31, 32]. The composition range of Ni–Si–Mn clusters to become brittle G-phase is a subject to be investigated further.

4. Crystal orientation relationship with the matrix

Crystal orientation relationship between precipitates and matrix is a potential factor controlling the mechanical properties of metals and alloys. Dislocations can glide on specific atomic planes, the choice of which is specific to crystal structure and material. For instance, the slip plane is the {111} plane for fcc metals, the {0001} plane for hcp magnesium, and the {10-10} plane for hcp titanium and hcp zirconium [9]. When the slip plane of precipitates is not parallel to that of the matrix, dislocations are in theory unable to cut through the precipitates. Although the orientation relationship has been extensively studied in the past [50], only a few studies have been reported on the effect of the crystal mismatch on the plasticity [1, 2]. The absence of such studies is partly due to a technical difficulty in determination of crystal orientation of fine precipitate particles as mentioned in the Section 2. Recently, Matsukawa et al. performed a systematic analysis on the parallelism of atomic planes between precipitates and matrix in a Zr–2.5Nb alloy: the precipitates are bcc Nb containing Zr ~10% and the matrix is hcp Zr. Based on the analysis results obtained from 100 precipitate particles (~50 nm in diameter) by means of TKD, they demonstrated that the orientation is practically random. Only 1 out of 100 precipitates had a slip plane parallel to that of the matrix. Their experimental result is inconsistent with a preceding theoretical prediction by Zhang and Kelly [51, 52]. Judging from the mismatch of inter-planar spacings, the most favorable crystal orientation relationship for the Nb-rich bcc precipitates in the hcp Zr matrix is $(\bar{1}011)$hcp$//(\bar{1}10)_{bcc} \wedge (11\bar{2}3)_{hcp}//(113)_{bcc}$ (**Figure 2**). Matsukawa et al. further demonstrated that the absence of such a specific crystal orientation relationship is attributable to the recrystallization of the matrix. In the Zr–2.5Nb alloy, precipitation occurs in parallel with recrystallization as follows. The Nb atoms are fully dissolved in the matrix at high temperatures with a bcc structure (**Figure 10**). Quenching from this temperature range results in nucleation of bcc Nb nano-precipitates and hcp Zr fine martensites. Ostwald ripening of Nb precipitates occurs during annealing at medium temperatures (773–853 K) together with the recrystallization of the martensite Zr matrix. The initial orientation relationship between the precipitates and the matrix is overwritten by the recrystallization.

In the study of the Zr–2.5Nb alloy, the parallelism of slip planes between precipitates and matrix was analyzed as follows. This analysis is achieved by using the Euler angles obtained from EBSD/TKD measurements, though so far not automated. The analysis procedure is slightly different depending on the analysis software due to the different definition of the Euler angles. In the case of the TSL-OIM software based on Bunge's description [53], the Euler angles $(\varphi_1, \Phi, \varphi_2)$ are given by three rotations along z_1-x-z_2 axes in accordance with passive rotation (intrinsic rotation), where the axes are rotated instead of the vectors of object, while the object is fixed in space (**Figure 11**). In this case, the rotation matrix (R) relative to the space coordinates is given as follows [54]:
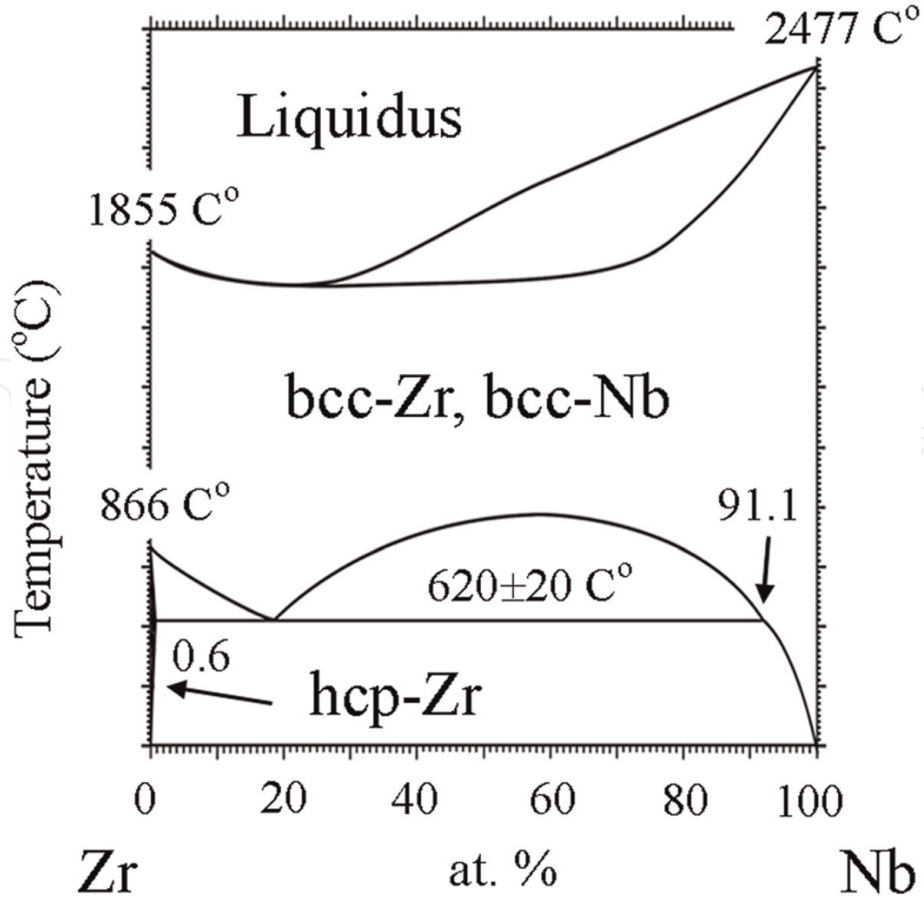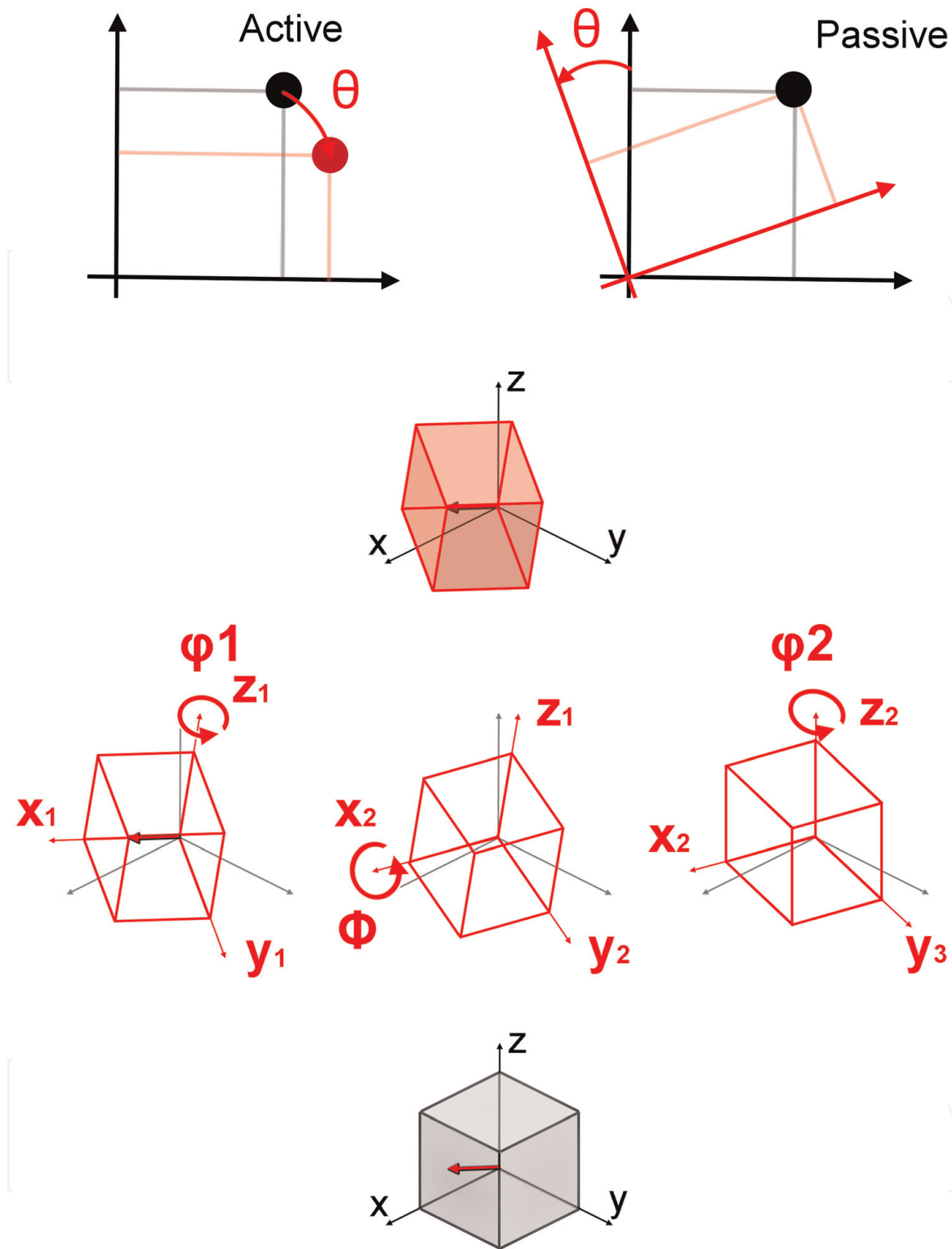
Figure 10
The Zr–Nb binary alloy phase diagram [14].

$$
R = R_{Z_2}(\varphi_2)R_x(\Phi)R_{Z_1}(\varphi_1) = \begin{pmatrix} \cos\varphi_2 & \sin\varphi_2 & 0 \\ -\sin\varphi_2 & \cos\varphi_2 & 0 \\ 0 & 0 & 1 \end{pmatrix} \begin{pmatrix} 1 & 0 & 0 \\ 0 & \cos\Phi & \sin\Phi \\ 0 & -\sin\Phi & \cos\Phi \end{pmatrix} \begin{pmatrix} \cos\varphi_1 & \sin\varphi_1 & 0 \\ -\sin\varphi_1 & \cos\varphi_1 & 0 \\ 0 & 0 & 1 \end{pmatrix}
$$

$$
= \begin{pmatrix} \cos\varphi_1\cos\varphi_2 - \sin\varphi_1\sin\varphi_2\cos\Phi & \sin\varphi_1\cos\varphi_2 + \cos\varphi_1\sin\varphi_2\cos\Phi & \sin\varphi_2\sin\Phi \\ -\cos\varphi_1\sin\varphi_2 - \sin\varphi_1\cos\varphi_2\cos\Phi & -\sin\varphi_1\sin\varphi_2 + \cos\varphi_1\cos\varphi_2\cos\Phi & \cos\varphi_2\sin\Phi \\ \sin\varphi_1\sin\Phi & -\cos\varphi_1\sin\Phi & \cos\Phi \end{pmatrix}
$$

$$(1)$$

In the reference crystal, the z- and the x-axes of space coordinates are parallel to the [001] and to the [100] directions of cubic crystals. Here, we consider the orientation relationship between two cubic crystals, A and B, whose rotation matrices relative to the reference crystal are R_A and R_B. The rotation matrix between these two crystals (R_C) is given as follows:

$$
\begin{pmatrix} H_1 \\ K_1 \\ L_1 \end{pmatrix} = R_A \begin{pmatrix} 0 \\ 0 \\ 1 \end{pmatrix} \rightarrow R_A^{-1} \begin{pmatrix} H_1 \\ K_1 \\ L_1 \end{pmatrix} = \begin{pmatrix} 0 \\ 0 \\ 1 \end{pmatrix} \tag{2}
$$

$$
\begin{pmatrix} H_2 \\ K_2 \\ L_2 \end{pmatrix} = R_B \begin{pmatrix} 0 \\ 0 \\ 1 \end{pmatrix} \rightarrow R_B^{-1} \begin{pmatrix} H_2 \\ K_2 \\ L_2 \end{pmatrix} = \begin{pmatrix} 0 \\ 0 \\ 1 \end{pmatrix} \tag{3}
$$

Figure 11
Passive rotations of a cubic crystal with Euler angles (the Bunge Euler angles).

$$\begin{pmatrix} 0 \\ 0 \\ 1 \end{pmatrix} = R_B^{-1} \begin{pmatrix} H_2 \\ K_2 \\ L_2 \end{pmatrix} = R_A^{-1} \begin{pmatrix} H_1 \\ K_1 \\ L_1 \end{pmatrix} \quad \rightarrow \quad \begin{pmatrix} H_2 \\ K_2 \\ L_2 \end{pmatrix} = R_B\, R_A^{-1} \begin{pmatrix} H_1 \\ K_1 \\ L_1 \end{pmatrix} \quad (4)$$

$$\begin{pmatrix} H_2 \\ K_2 \\ L_2 \end{pmatrix} = R_C \begin{pmatrix} H_1 \\ K_1 \\ L_1 \end{pmatrix} \quad \rightarrow \quad R_C = R_B\, R_A^{-1} \quad (5)$$

An atomic plane of crystal B, $(H_2' \, K_2' \, L_2')$, parallel to $(H_1' \, K_1' \, L_1')$ of the crystal A is expressed by using the Euler rotation matrix R_D, which rotates the sample coordinates in such a way as to match $[H_1' \, K_1' \, L_1']$ to $[001]$ in the space coordinates:

$$\begin{pmatrix} H_1' \\ K_1' \\ L_1' \end{pmatrix} = R_D \begin{pmatrix} 0 \\ 0 \\ 1 \end{pmatrix} \quad \rightarrow \quad \begin{pmatrix} H_2' \\ K_2' \\ L_2' \end{pmatrix} = R_B \, R_A{}^{-1} \begin{pmatrix} H_1' \\ K_1' \\ L_1' \end{pmatrix} = R_B \, R_A{}^{-1} R_D \begin{pmatrix} 0 \\ 0 \\ 1 \end{pmatrix}$$

(6)

R_A and R_B are directly determined by EBSD measurements of crystals A and B. The Euler angles of the R_D are determined by using a simulation equipped on the TSL-OIM data collection software. This simulation module is capable of (1) calculating how the index of a crystal (in the ND and the RD directions) changes in accordance with rotations along the three axes and (2) visualizing where the index (of the ND direction) is located on the Kikuchi map (the inverse pole figure). By using these functions, the index $(H_2' \, K_2' \, L_2')$ of precipitate particles can be plotted on one inverse pole figure, though plotting the data points is a time-consuming hand work.

Determination of theoretical accuracy of this analysis method is not straightforward, since errors are introduced by various factors such as (1) the conversion of the Euler angles $(\varphi_1, \Phi, \varphi_2)$ to direction cosines, (2) the conversion of direction cosines denoted in fractional values to the Millar indices (h k l) denoted in integer ratio, and (3) the noise of EBSD data. In order to estimate the practical accuracy of this analysis method, they first analyzed a standard sample in which the atomic-plane parallelism between grains is already known. Their standard sample was a type-316 austenitic stainless steel containing annealing twins (**Figure 12**). The twin boundary of fcc metals is one of the four crystallographically equivalent {111} planes. The Euler angles of these {111} planes for the R_D rotation are, e.g., $(\varphi_1, \Phi, \varphi_2)$ = (0°, 55°, 45°), (0°, 55°, 135°), (0°, 55°, 225°), and (0°, 55°, 315°). They performed this analysis on 50 twin couples and found that the largest offset from the exact {111} was 3.3°. This is the magnitude of practical error of this analysis method.

To date, several orientation relationships have been reported on bcc precipitates in hcp matrix (**Figure 13**). The parallelism of slip planes in those orientation relationships is as follows: (1) the Burgers orientation relationship [13]: $(0001)_{hcp}$//$(110)_{bcc} \wedge (2\bar{1}\bar{1}0)_{hcp}$//$(1\bar{1}1)_{bcc}$. The slip plane of hcp Zr matrix, $\{10\bar{1}0\}$, is not exactly parallel to the slip plane of bcc Nb precipitates, {110} or {112}; however, the rotational offset between the $(1\bar{1}0)_{bcc}$ and the $(1\bar{1}00)_{hcp}$ is only 5.3°. (2) The Pitsch-Schrader orientation relationship [55]: $(0001)_{hcp}$//$(110)_{bcc} \wedge (1\bar{1}00)_{hcp}$//$(1\bar{1}0)_{bcc}$. The slip planes are exactly parallel to each other. (3) The Potter orientation relationship [56]: $(2\bar{1}\bar{1}0)_{hcp}$//$(1\bar{1}1)_{bcc}, \wedge (1\bar{1}01)_{hcp}$//$(011)_{bcc}$. One of the $\{112\}_{bcc}$ is not exactly but nearly parallel to one of the $\{1\bar{1}00\}_{hcp}$. This orientation relationship is close to the Burgers, from which the rotational offset is only $\sim$1.5°. (4) The Rong-Dunlop orientation relationship [57]: $(0001)_{hcp}$//$(120)_{bcc} \wedge (11\bar{2}0)_{hcp}$//$(001)_{bcc} \wedge (1\bar{1}00)_{hcp}$//$(2\bar{1}0)_{bcc}$. The slip plane of hcp and bcc crystals is not parallel to each other. (5) The Zhang and Kelly orientation relationships [51, 52]: $(0001)_{hcp}$//$(\bar{1}10)_{bcc} \wedge (10\bar{1}0)_{hcp}$//$(113)_{bcc}$. They proposed several orientation relationships. This one is the most favorable orientation relationship for the bcc Nb precipitates, in terms of the mismatch of the lattice parameter. Their analysis also
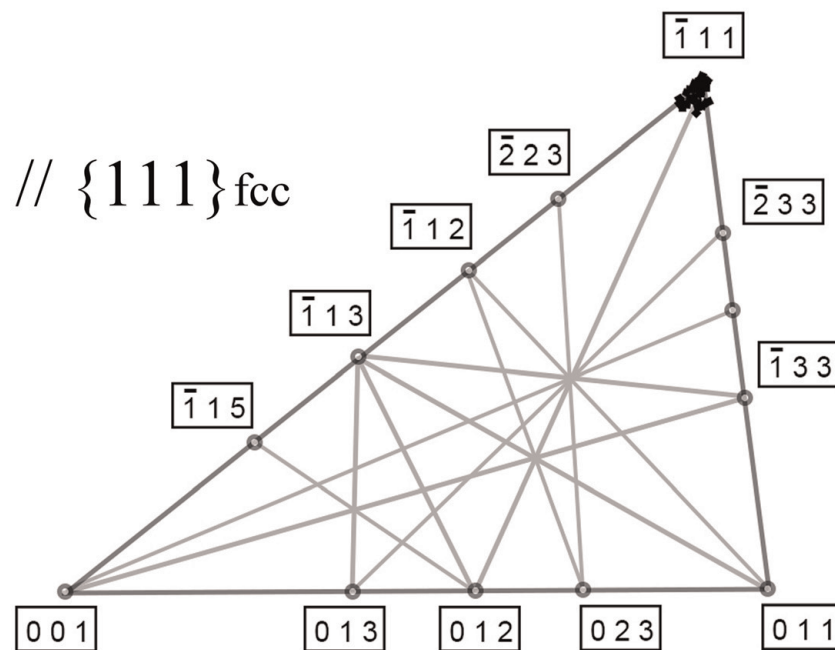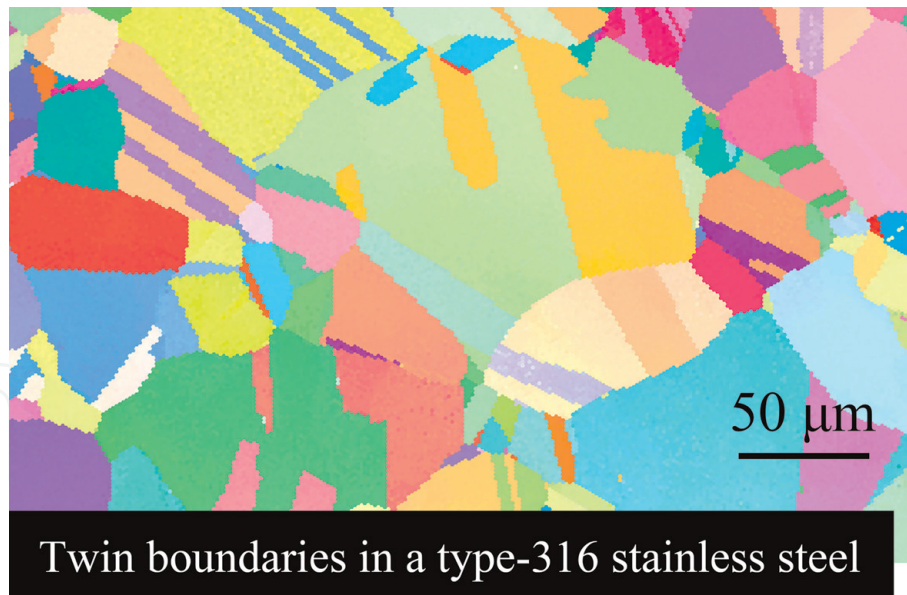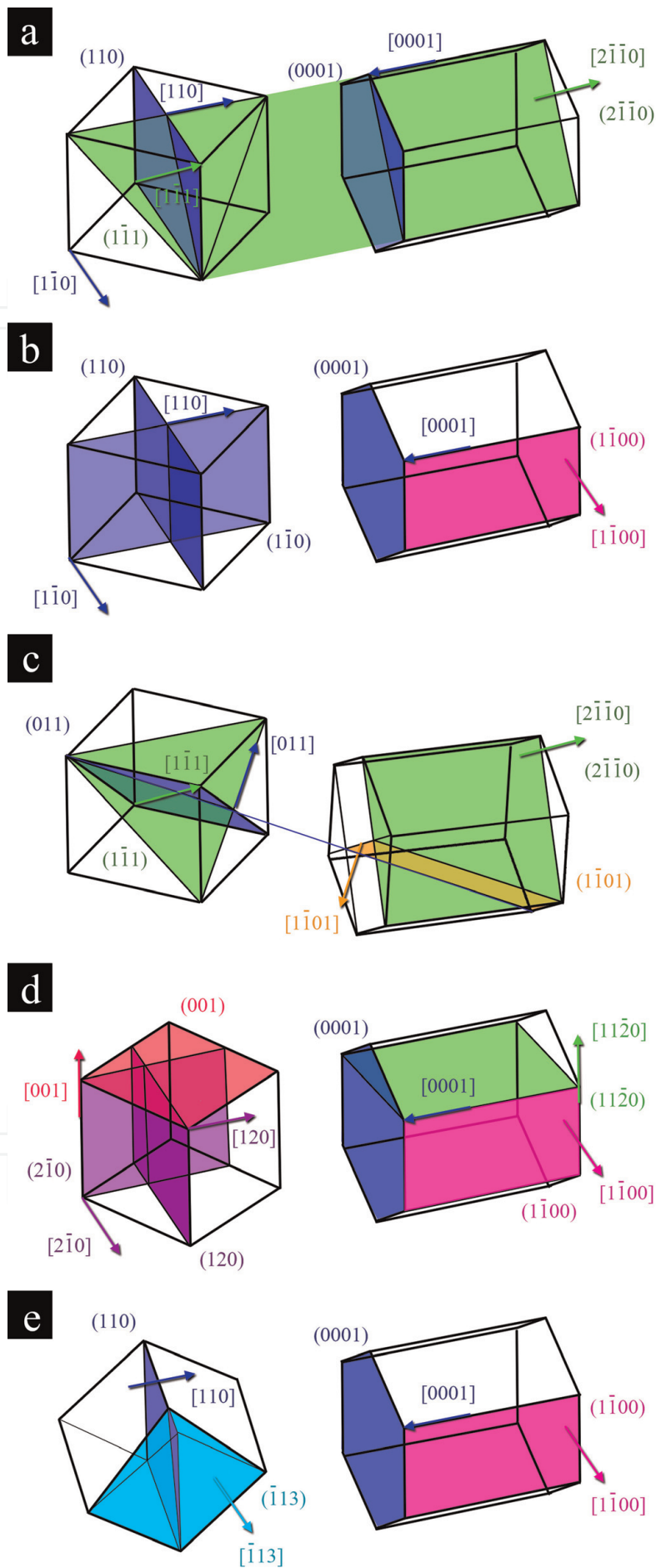
Figure 12
Evaluation of the magnitude of error of the EBSD analysis method on the atomic plane parallelism described in this chapter, using annealing twins in a type-316 stainless steel [2]. The largest offset from the exact {111} was ∼3.3°. This is considered as the magnitude of practical error of this analysis method.

suggested that the Pitsch-Schrader and the Rong-Dunlop orientation relationships are favorable over the Burgers orientation relationship for Nb-rich precipitates. This orientation relationship is close to the Burgers, and the slip plane of matrix is not exactly parallel to that of precipitates.

The magnitude of error of the abovementioned analysis of atomic-plane parallelism is greater than the orientation difference between the Potter and the Burgers orientation relationships, 1.5°. It follows that these two orientation relationships are practically indistinguishable from each other in this analysis. On the other hand, the orientation difference between the Pitsch-Schrader and the Burgers orientation relationships is 5.3°; in theory, they are distinguishable. In both the Burgers and the Pitsch-Schrader orientation relationships, the basal plane of the hcp crystal is parallel to a {110} plane of the bcc crystal. In other words, when any one of {110} planes of a precipitate is not parallel to the (0001) plane of the matrix, it follows that the precipitate is in neither one of these two orientation relationships. The criterion for the judgment of whether the Burgers or the Pitsch-Schrader is given by

Figure 13
Examples of crystal orientation relationships between bcc and hcp crystals [2]: (a) the Burgers, (b) the Pitsch-Schrader, (c) the Potter, (d) the Rong-Dunlop, and (e) the Zhang-Kelly No. 5.

	Index	Euler angle (φ_1, Φ, φ_2) [°]
Basal	0001	0, 0, 0
Prismatic (type 1)	01$\bar{1}$0	0, 90, 0
	10$\bar{1}$0	0, 90, 60
	1$\bar{1}$00	0, 90, 120
Prismatic (type 2)	2$\bar{1}\bar{1}$0	0, 90, 90
	1$\bar{2}$10	0, 90, 150
	$\bar{1}\bar{1}$20	0, 90, 210

Table 1
The Euler angles to rotate the object coordinates of an hcp crystal in such a way that the plane of interest coincide with the (0001) of the reference hcp crystal, whose [0001] and $[2\bar{1}\bar{1}0]$ are parallel to ND and RD, respectively.

another atomic-plane parallelism, which is whether $\{11\bar{2}0\}_{hcp}//\{111\}_{bcc}$ or $\{1\bar{1}00\}_{hcp}//\{110\}_{bcc}$. As for the parallelism of slip planes, hcp crystals have three crystallographically equivalent $\{10\bar{1}0\}$ planes, whereas bcc crystals have 12 equivalent $\{110\}$ planes and another 12 equivalent $\{112\}$ planes.

In the study of the Zr–2.5Nb alloy, Matsukawa et al. fixed the plane of hcp matrix and plotted its corresponding atomic planes of bcc precipitates on an inverse pole figure (**Figure 4**). In the TSL-OIM software, the Euler angles of hcp crystals are given in the orthogonal coordinate system. In the reference crystal, the z- and the x-axes of space coordinates are parallel to the $[0001]_{hcp}$ and the $[2\bar{1}\bar{1}0]_{hcp}$, respectively. The Euler angles for the RD rotation of the $\{11\bar{2}0\}$ and the $\{10\bar{1}0\}$ planes are shown in **Table 1**.

5. Conclusion

Recent progresses in our understanding of the crystallography of precipitates in metals and alloys have been briefly reviewed. The major highlights are the following three: (1) crystal structure of precipitates changes during nucleation. This concept in itself has been known since the 1930s. Recent new findings concern the critical conditions for the structural change in terms of fluctuations in size and composition, discovered by mean of combining transmission electron microscopy crystallographic analysis with atom probe tomography compositional analysis. It appears that the structural change occurs at a critical size with a critical composition. There is a long incubation period (in some cases a year long) before the structural change after the growth to be the critical size. During the incubation period, enrichment of solute elements occurs inside the precipitates without further size growth. It still remains unclear if these features are universal for any types of precipitates. This research field is expected to advance drastically in the years ahead. (2) In the past years, it has also become technically possible to examine the crystal orientation relationship of fine precipitate particles such as ~50 nm in diameter with the matrix, on numbers of samples numerically sufficient for statistical arguments. Transmission Kikuchi diffraction, which is an advanced technique of electron backscatter diffraction equipped with a scanning electron microscope, revealed that the crystal orientation of precipitates can be random even when they are in theory favorable to have a specific orientation relationship with the matrix from the viewpoint of lattice mismatch. It appears that such a situation is realized when the

matrix exhibits recrystallization after precipitation. (3) Crystal orientation relationship between precipitates and matrix was found to be a factor controlling the magnitude of precipitation hardening. This is a new concept beyond the scope of the traditional theory of precipitation hardening, which assumes that the hardening is controlled solely by the shear modulus, whether or not the precipitates are harder than the matrix. In cases where the slip plane of precipitates is not parallel to the slip plane of the matrix, dislocations gliding in the matrix are unable to cut through them, resulting in strong obstacles regardless of the shear modulus. Further information on this issue is provided in the next chapter.

Acknowledgements

Conflict of interest

The author declares no conflicts of interest directly relevant to the content of this chapter.

Author details

Yoshitaka Matsukawa[1,2*]

1 Division of Materials Science, Faculty of Advanced Science and Technology, Kumamoto University, Kumamoto, Japan

2 Institute for Materials Research, Tohoku University, Sendai, Japan

*Address all correspondence to: ym2@msre.kumamoto-u.ac.jp

IntechOpen

References

[1] Matsukawa Y, Yang HL, Saito K, Murakami Y, Maruyama T, Iwai T, et al. The effect of crystallographic mismatch on the obstacle strength of second phase precipitate particles in dispersion strengthening: Bcc Nb particles and nanometric Nb clusters embedded in hcp Zr. Acta Materialia. 2016;**102**: 323-332

[2] Matsukawa Y, Okuma I, Muta H, Shinohara Y, Suzue R, Yang HL, et al. Crystallographic analysis on atomic-plane parallelisms between bcc precipitates and hcp matrix in recrystallized Zr–2.5Nb alloys. Acta Materialia. 2017;**126**:86-101

[3] Matsukawa Y, Takeuchi T, Kakubo Y, Suzudo T, Watanabe H, Abe H, et al. The two-step nucleation of G-phase in ferrite. Acta Materialia. 2016;**116**: 104-113

[4] Gibbs JW. On the equilibrium of heterogeneous substances. Transactions Connecticut Academy of Arts and Sciences;**3**(1876):108-248

[5] Orowan E, Zur KI. Zeitschrift für Physik. 1934;**89**:605-613

[6] Polanyi M. Über eine Art Gitterstörung, die einen Kristall plastisch machen könnte. Zeitschrift für Physik. 1934;**89**:660-664

[7] Taylor GI. The mechanism of plastic deformation of crystals. Part I.—Theoretical. Proceedings of the Royal Society of London. Series A. 1934;**145**: 362-387

[8] Hirth JP. A brief history of dislocation theory. Metallurgical Transactions A. 1985;**16A**:2085-2090

[9] Bacon DJ, Osetsky YN, Rodney D. Dislocation–obstacle interactions at the atomic level. In: Hirth JP, Kubin L, editors. Dislocations in Solids.

Amsterdam: Elsevier; 2009. pp. 75, 85–136, 228–237

[10] Orowan E. Discussion. In: Symposium on Internal Stresses in Metals and Alloys, Institute of Metals Monograph and Report Series. Vol. 5. London: Institute of Metals; 1948. pp. 451-453

[11] Ardell AJ. Precipitation hardening. Metallurgical Transactions A. 1985;**16A**: 2131-2165

[12] Mehrer H. Diffusion in Solids. Springer Series Solid State Science. Vol. 155. Berlin; 2007. pp. 297-338

[13] Burgers WG. On the process of transition of the cubic-body-centered modification into the hexagonal-close-packed modification of zirconium. Physica. 1934;**1**:26-586

[14] Okamoto H. Nb–Zr. Journal of Phase Equilibria. 1992;**13**:577-577

[15] Rogers BA, Atkins DF. Zirconium-clumbium diagram. Transactions of AIME. 1944;**203**:1034-1041

[16] Rietveld HM. The rietveld method—A historical perspective. Australian Physics. 1988;**41**:113-116

[17] Yang HL, Shen JJ, Kano S, Matsukawa Y, Li YF, Satoh Y, et al. Effects of Mo addition on precipitation in Zr–1.2Nb alloys. Materials Letters. 2015;**158**:88-91

[18] Tanigawa H, Sakasegawa H, Klueh RL. Irradiation effects on precipitation in reduced-activation ferritic/martensitic steels. Metallurgical Transactions. 2005;**46**:469-474

[19] Buseck PR, Iijima S. High resolution electron microscopy of silicates. American Mineralogist. 1974;**59**:1-21

[20] Rauch EF, Portillo J, Nicolopoulos S, Bultreys D, Rouvimov S, Moeck P. Automated nanocrystal orientation and phase mapping in the transmission electron microscope on the basis of precession electron diffraction. Zeitschrift für Kristallographie. 2010;**225**:103-109

[21] Viladot D, Véron M, Gemmi M, Peiró F, Portillo J, Estradé S, et al. Orientation and phase mapping in the transmission electron microscope using precession-assisted diffraction spot recognition: State-of-the-art results. Journal of Microscopy. 2013;**252**:23-34

[22] Williams DB, Carter CB. Transmission Electron Microscopy. New York: Springer; 1996. pp. 291-299

[23] Zaefferer S. A critical review of orientation microscopy in SEM and TEM. Crystal Research and Technology. 2011;**46**:607-628

[24] Trimby PW. Orientation mapping of nanostructured materials using transmission Kikuchi diffraction in the scanning electron microscope. Ultramicroscopy. 2012;**120**:16-24

[25] Rice KP, Keller RR, Stoykovich MP. Specimen-thickness effects on transmission Kikuchi patterns in the scanning electron microscope. Journal of Microscopy. 2014;**254**:129-136

[26] Hirsch PB, Howie A, Whelan MJ. Electron microscopy of thin metals. 2nd ed. Malabar: R.E. Krieger Publishing Company; 1977. pp. 119-121

[27] Gault B, Moody MP, Cairney JM, Ringer SP. Atom probe tomography. In: Springer Series in Materials Science. Vol. 160. New York: Springer; 2011. pp. 185-190

[28] Miller MK, Cerezo A, Hetherington MG, Smith GDW. Atom probe field ion microscopy. In: Monographs on the Physics and Chemistry of Materials. Vol. 52. Oxford: Oxford Science Publications; 1999. pp. 191-199

[29] Blavette D, Vurpillot F, Pareige P, Menand A. A model accounting for spatial overlaps in 3Datom-probe microscopy. Ultramicroscopy. 2001;**89**: 145-153

[30] Vurpillot F, Bostel A, Blavette D. Trajectory overlaps and local magnification in three-dimensional atom probe. Applied Physics Letters. 2000;**76**:3127-3129

[31] Kuramoto A, Toyama T, Takeuchi T, Nagai a Y, Hasegawa M, Yoshiie T, et al. Post-irradiation annealing behavior of microstructure and hardening of a reactor pressure vessel steel studied by positron annihilation and atom probe tomography. Journal of Nuclear Materials. 2012;**425**:65-70

[32] Kuramoto A, Toyama T, Nagai Y, Inoue K, Nozawa Y, Hasegawa M, et al. Microstructural changes in a Russian-type reactor weld material after neutron irradiation, post-irradiation annealing and re-irradiation studied by atom probe tomography and positron annihilation spectroscopy. Acta Materialia. 2013;**61**:5236-5246

[33] Erdemir D, Lee AY, Myerson AS. Nucleation of crystals from solution: Classical and two step models. Accounts of Chemical Research. 2009;**42**:621-629

[34] Peng Y, Wang F, Wang Z, Alsayed AM, Zhang Z, Yodh AG, et al. Two-step nucleation mechanism in solid–solid phase transitions. Nature Materials. 2014;**14**:101-108

[35] Borelius G. Zur theorie der umwandlungen von metallischen mischphasen. Annals of Physics. 1937; **28**:507-519

[36] Hobstetter JN. Stable transformation nuclei in solids. Transactions of the AIME. 1949;**180**:12130

[37] Ostwald W. The formation and changes of solids (Translated from German). Zeitschrift für Physikalische Chemie. 1897;**22**:289-330

[38] Chung SY, Kim YM, Kim JG, Kim YJ. Multiphase transformation and Ostwald's rule of stages during crystallization of a metal phosphate. Nature Physics. 2009;**5**:68-73

[39] Biswas A, Siegel DJ, Wolverton C, Seidman DN. Precipitates in Al–Cu alloys revisited: Atom-probe tomographic experiments and first-principles calculations of compositional evolution and interfacial segregation. Acta Materialia. 2011;**59**:6187-6204

[40] Marceau RKH, Sha G, Ferragut R, Dupasquier A, Ringer SP. Solute clustering in Al–Cu–Mg alloys during the early stages of elevated temperature ageing. Acta Materialia. 2010;**58**: 4923-4939

[41] Othen PJ, Jenkins ML, Smith DW. High-resolution electron microscopy studies of the structure of Cu precipitates in α-Fe. Philosophical Magazine: A. 1994;**70**:1-24

[42] Mateo A, Llanes L, Anglada M, Redjaimia A, Metauer G. Characterization of the intermetallic G-phase in an AISI 329 duplex stainless steel. Journal of Materials Science. 1997; **32**:4533-4540

[43] Miller MK, Bentley J. APFIM and AEM investigation of CF8 and CF8M primary coolant pipe steels. Journal of Materials Science and Technology. 1990;**6**:285-292

[44] Zinkle SJ, Was GS. Materials challenges in nuclear energy. Acta Materialia. 2013;**61**:735-758

[45] Odette GR, Wirth BD. A computational microscopy study of nanostructural evolution in irradiated pressure vessel steels. Journal of Nuclear Materials. 1997;**251**:157-171

[46] Soneda N. In: Soneda N, editor. Irradiation Embrittlement of Reactor Pressure VesselsEmbrittlement correlation methods to identify trends in embrittlement in reactor pressure vessels (RPVs). Cambridge: Woodhead Publ Ltd; 2015. pp. 333-377

[47] Ngayam-Happy R, Becquart CS, Domain C, Malerba L. Formation and evolution of MnNi clusters in neutron irradiated dilute Fe alloys modelled by a first principle-based AKMC method. Journal of Nuclear Materials. 2012;**426**: 198-207

[48] Wells PB, Yamamoto T, Miller B, Milot T, Cole J, Wu Y, et al. Evolution of manganese–nickel–silicon-dominated phases in highly irradiated reactor pressure vessel steels. Acta Materialia. 2014;**80**:205-219

[49] Sprouster DJ, Sinsheimer J, Dooryhee E, Ghose SK, Wells P, Stan T, et al. Structural characterization of nanoscale intermetallic precipitates in highly neutron irradiated reactor pressure vessel steels. Scripta Materialia. 2016;**113**:18-22

[50] Dahmen U. Orientation relationships in precipitation systems. Acta Metallurgica. 1982;**30**:63-73

[51] Zhang M-X, Kelly PM. Crystallographic features of phase transformations in solids. Progress in Materials Science. 2009;**54**: 1101-1170

[52] Zhang M-X, Kelly PM. Edge-to-edge matching and its applications: Part I. Application to the simple HCP/BCC system. Acta Materialia. 2005;**53**: 1073-1084

[53] Bunge H-J. Texture Analysis in Materials Science: Mathematical

Methods. English ed. London:
Butterworth; 1982. pp. 4-22

[54] Engler O, Landle V. Introduction to
Texture Analysis. 2nd ed. New York:
CRC Press; 2010. pp. 33-36

[55] Pitsch W, Schrader A. Die
ausscheidungsform des ε-karbids im
ferrit und im martensit beim anlassen.
Archiv fur das Eisenhuttenwesen. 1958;
29:715-721

[56] Potter DL. The structure,
morphology and orientation
relationship of V_3N in α-vanadium.
Journal of the Less Common Metals.
1973;**31**:299-309

[57] Rong W, Dunlop GL. The
crystallography of secondary carbide
precipitation in high speed steel. Acta
Metallurgica. 1984;**32**:1591-1599